INITIAL PETROGRAPHIC ANALYSIS OF APOLLO 17 73002 CONTINUOUS CORE THIN SECTIONS USING QEMSCAN MAPPING TECHNIQUES. S. K. Bell[1], K. H. Joy[1], M. Nottingham[1], R. Tartèse[1], R. H. Jones[1], J. J. Kent[2] and C.K. Shearer[3,4] and the ANGSA science team[5]. [1]Department of Earth and Environmental Sciences, University of Manchester, Oxford Road, Manchester, M19 3PL, UK (samantha.bell@manchester.ac.uk), [2]GeoControl Systems Inc., Jacobs JETS Contract, NASA/JSC, [3]Dept. of Earth and Planetary Science, Institute of Meteoritics, University of New Mexico, Albuquerque, New Mexico 87131, [4]Lunar and Planetary Institute, Houston TX 77058, [5]ANGSA Science Team list at https://www.lpi.usra.edu/ ANGSA /teams/.

Introduction: In 1972, the Apollo 17 mission landed in the Taurus-Littrow Valley located in the southeastern edge of Mare Serenitatis [1]. During EVA 2 at Station 3, a double drive tube was used to collect a sealed core sample (73001/2) of the upper ~70 cm of the lunar regolith [2-4]. The core was taken from the surface of the light mantle deposit, found at the base of the South Massif [3]. For nearly 50 years, the sealed core samples have remained unopened. This study is part of the Apollo Next Generation Sample Analysis (ANGSA) initiative to analyze the continuous thin sections from the Apollo 17 drive tubes opened in 2019 [5-7].

Methods: Quantitative Evaluation of Minerals by SCANing electron microscopy (QEMSCAN) is a non-destructive system of automated quantitative petrology that can produce mineral phase identification maps and qualitative element maps [8,9]. As such, QEMSCAN is a valuable method for extracting a large amount of information about the mineralogical diversity of the Apollo 17 continuous core sections. Here we present the preliminary petrographic analysis of QEMSCAN data for thin sections 73002,6011, 73002,6012, 73002,6013 and 73002,6014, representing sampling depths of 0-4.7, 4.8-9.5, 9.6-14.2 and 14.3-18.4 cm.

Thin sections were prepared and imaged optically using plane-polarized, cross-polarized, and reflected light (Fig. 1a-b) at the NASA Johnson Space Center Apollo Curatorial labs. Samples were then analyzed using an FEI QUANTA 650 field emission gun (FEG) scanning electron microscope (SEM) at the University of Manchester, equipped with a single Bruker XFlash energy dispersive X-ray spectrometer (EDS). The FEI QEMSCAN operates using an accelerating voltage of 25 kV and a 10 nA beam current. Samples were analyzed using field image mode with a step size (i.e. pixel size) of 5 µm. The software uses a Species Identification Protocol (SIP) list to assign a mineral to each pixel based on the EDS spectra and BSE brightness collected at each individual point. Samples were classified using a modified version of a SIP list specifically established for lunar samples [8]. As well as mineral phase maps, backscattered electron (BSE), and elemental maps were also exported from the QEMSCAN datasets (Fig. 1).

QEMSCAN data processing: All maps were initially classified in the iExplorer QEMSCAN software using our lunar specific SIP list. Additional secondary SIP lists were established to view the data in a number of useful ways including grouping SIP entries into broad mineral groups (i.e. augite, pigeonite, enstatite, etc. under the phase name "pyroxene") and to pinpoint specific minerals of interest, such as zircon or phosphate grains for potential age dating.

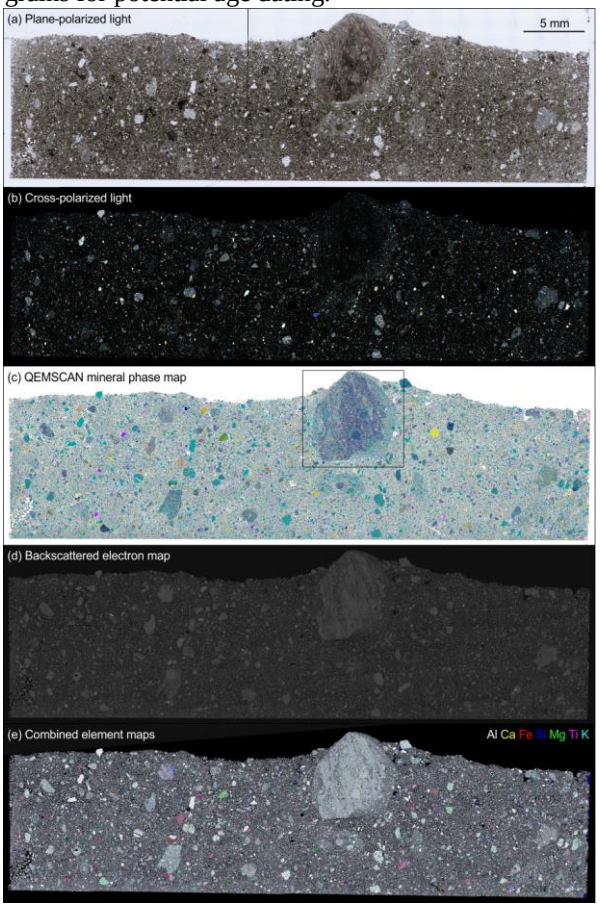

Figure 1: *(a-b) Optical microscope images of 73002,6011. (c) QEMSCAN mineral and phase map using full lunar SIP list (broadly, colors are: feldspar = blue/turquoise, pyroxene = purples, olivine = green, yellow = volcanic glass bead), with box highlighting a large clast. (d) QEMSCAN generated BSE map. (e) Combined false-color element map. Scale bar in (a) applies to all images.*

The QEMSCAN software also contains a number of processors, filters, and formulas that can be applied to the data to determine different properties. Here we used

the "area % of sample" function to provide an estimate of the modal mineralogy of the samples.

Results: The maximum clast size in the samples is ~8 mm, and the sections are dominated by the < 0.5 mm lithic clast and mineral size fraction. Lithic clasts include impact melt breccias with a wide range of textures, polymict lithic breccias, small fragments of mare basalt, agglutinates, along with glass spherules.

QEMSCAN phase, BSE, and elemental maps have been processed for all four thin sections in this study. In Figure 1c, a mineral phase map of 73002,6011 is shown, as an example. These phase maps are able to identify the multiple types of clasts in the samples, as well as glassy components (including volcanic glass or impact glass beads), and mineral fragments. Modal mineralogies of the major phases in each sample derived from these phase maps are shown in Figure 2. The proportions of olivine (~5-6%), pyroxene (~6.5-7.5%) and ilmenite (~1-1.5%) remain relatively consistent across the four thin sections (and in turn with core depth from 0 to 18.4 cm); a feature also noted by multispectral imaging studies of FeO and TiO_2 content along the core [9]. However, the proportion of plagioclase gradually increases with depth within the core from ~27% at 0-4.7 cm depth to 36% at 14.3-18.4 cm depths. This suggests a decrease in the amount of mafic material (i.e., mare basalt-derived clasts and minerals) and an increase of the amount of feldspathic material sampled with depth. The proportion of glass (a collective group including SIP entries for mafic glass, feldspathic glass, KREEP glass, and volcanic glass bead compositions) gradually decreases with depth within the core from ~52% to ~43%. The normalized abundances of plagioclase, olivine, and pyroxene in all four samples is comparable to mineral modal abundances obtained by spectral imagining of 73002 [10] and XRD analysis of other Station 3 Apollo 17 soils [11].

We note that as we have not yet undertaken an analysis looking at specific grain size ranges, it may also be possible that the variation in modal phase proportions across the thin sections could be skewed due to a few larger glass or plagioclase-rich clasts in some samples compared to others (e.g. the large dark blue clast of feldspathic glass in 73002,6011, as highlighted in Fig. 1c). However, the increase in plagioclase abundance with depth is similar to observations made by other techniques that have analyzed the 73002 drive core, which suggest that the quantity of mare basalt components decreases with depth [12], and that the reflectance spectral signature (i.e., as a measure of feldspathic phases ([5] and refs therein) increases with depth. Likewise the decrease in glass content with depth (Fig. 2) is consistent with the observation ([5] and refs therein) that the 73002 is more mature and submature (i.e., glass-rich) in the upper 10-15 cm portion of the core (as represented here by sections 6011-6013), compared with the lower portion of the core (as represented here by section 6014).

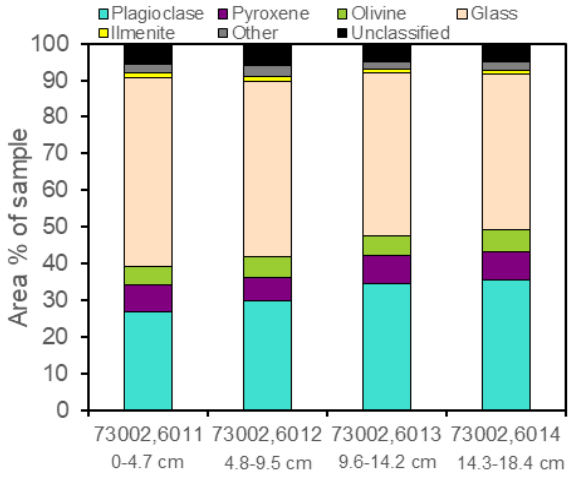

Figure 2: *Modal proportions of major phases in each of the four thin sections from core 73002, determined using QEMSCAN phase mapping data. 'Other' includes accessory minerals such as spinel or silica.*

Summary and future work: QEMSCAN provides a non-destructive method of collecting a wealth of mineralogical and textural data from the Apollo 17 ANGSA samples. Here we show how one of the many processors in the QEMSCAN software can be used to extract mineral phase proportions from 73002. Through further processing of the data collected, we will determine additional regolith properties (e.g. grain size and clast type / abundance), and use the methods developed to identify potential exogenously-derived components within the Apollo 17 regolith.

Acknowledgments: We thank the NASA JSC curatorial teams for preparing the continuous core sections. UoM research was supported by grants URF\R\201009 and STFC ST/M001253/1. CKS activities were supported by NASA Apollo Next Generation Sample Analysis Program (ANGSA) 80NSSC19K0958, University of New Mexico, and Lunar and Planetary Institute.

References: [1] Muehlberger W.R. et al. (1973) *USGS*, 6-91 [2] Jolliff B.L. et al. (2020) *51st LPSC*, Abstract #1970 [3] Wolfe E.W. et al. (1981) *USGS Prof. Paper, 1080*, 280 [4] Meyer C. (2011) *73001- Lunar Sample Comp.* [5] Shearer et al. (2022) *53rd LPSC abstract*, in press [6] Petro N.E. (2020) AGU, Abstract V017-01 [7] Simon S. et al. (2020) *AGU*, Abstract V013-0002 [8] Bell S.K. et al (2020), *J.Pet., 61*(4) [9] Valenzuela M. et al. (2021) *LPI Cont.*, #2609 [10] Sun L. et al. (2021) *MAPS*, 56(8), 1574-1584 [11] Taylor G. J. et al. (2019) *GCA*, 266, 17–28 [12] Neuman M.D. et al. (2021) *52nd LPSC*, Abstract # 1470.